SUPPLEMENTARY INFORMATION

Interleukin-2 druggability is modulated by global conformational transitions controlled by a helical capping switch

AUTHORS

Viviane S. De Paula[1], Kevin Jude[3-5], Santrupti Nerli[2], Caleb R. Glassman[3-5], Christopher Garcia[3-5], Nikolaos G. Sgourakis[1*]

[1] Department of Chemistry and Biochemistry, University of California Santa Cruz, Santa Cruz, California, USA.

[2]Department of Computer Science, University of California Santa Cruz, Santa Cruz, California, USA.

[3]Howard Hughes Medical Institute, Stanford University School of Medicine, Stanford, California, USA.

[4]Department of Molecular and Cellular Physiology, Stanford University School of Medicine, Stanford, California, USA.

[5]Department of Structural Biology, Stanford University School of Medicine, Stanford, California, USA.

www.pnas.org/cgi/doi/10.1073/pnas.2000419117

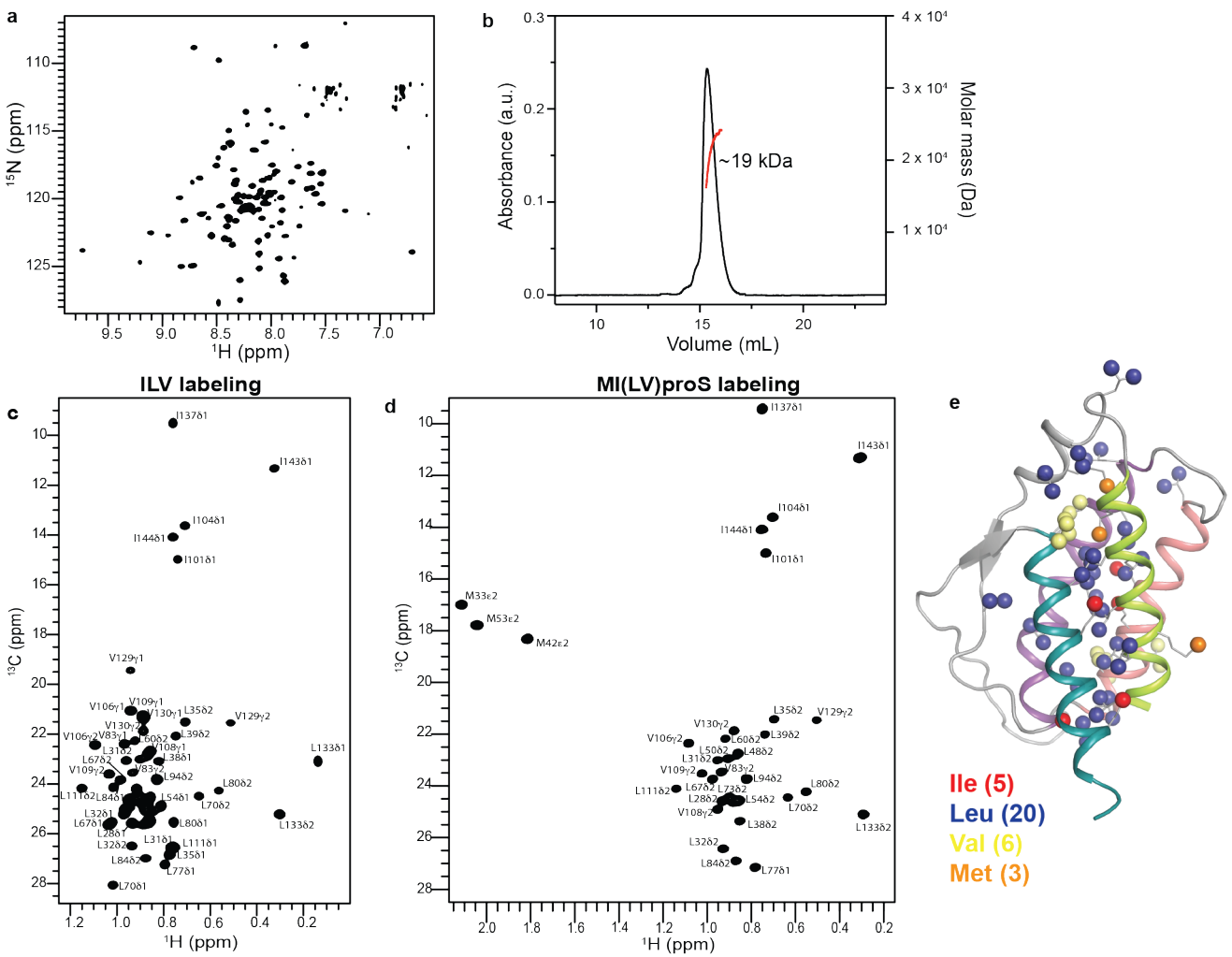

Supplementary Fig. 1 | NMR spectra of free mIL-2. (**a**) ^{1}H-^{15}N TROSY HSQC, (**c**) ^{1}H-^{13}C methyl HMQC spectra of [U-^{2}H,^{15}N, Ileδ$_1$-^{13}CH$_3$; Leu, Val-^{13}CH$_3$/^{12}CD$_3$] and (**d**) ^{1}H-^{13}C methyl HMQC spectra of [U-^{2}H,^{15}N, Iδ$_1$-^{13}CH$_3$, Mε,-^{13}CH$_3$, L, V proS]-labeled mIL-2 acquired at 800 MHz, 25 ºC. (**b**) MALS of free WT mIL-2 shows that the protein is monomeric in solution. (**e**) Distribution of assigned MILV methyl probes in the free mIL-2 structure. The backbone of the mIL-2 is show as in Figure 1. Color-coding: Ile, red; Leu, blue; Val, yellow; Met, orange. The numbers in parenthesis indicate the number of the corresponding residues in mIL-2.

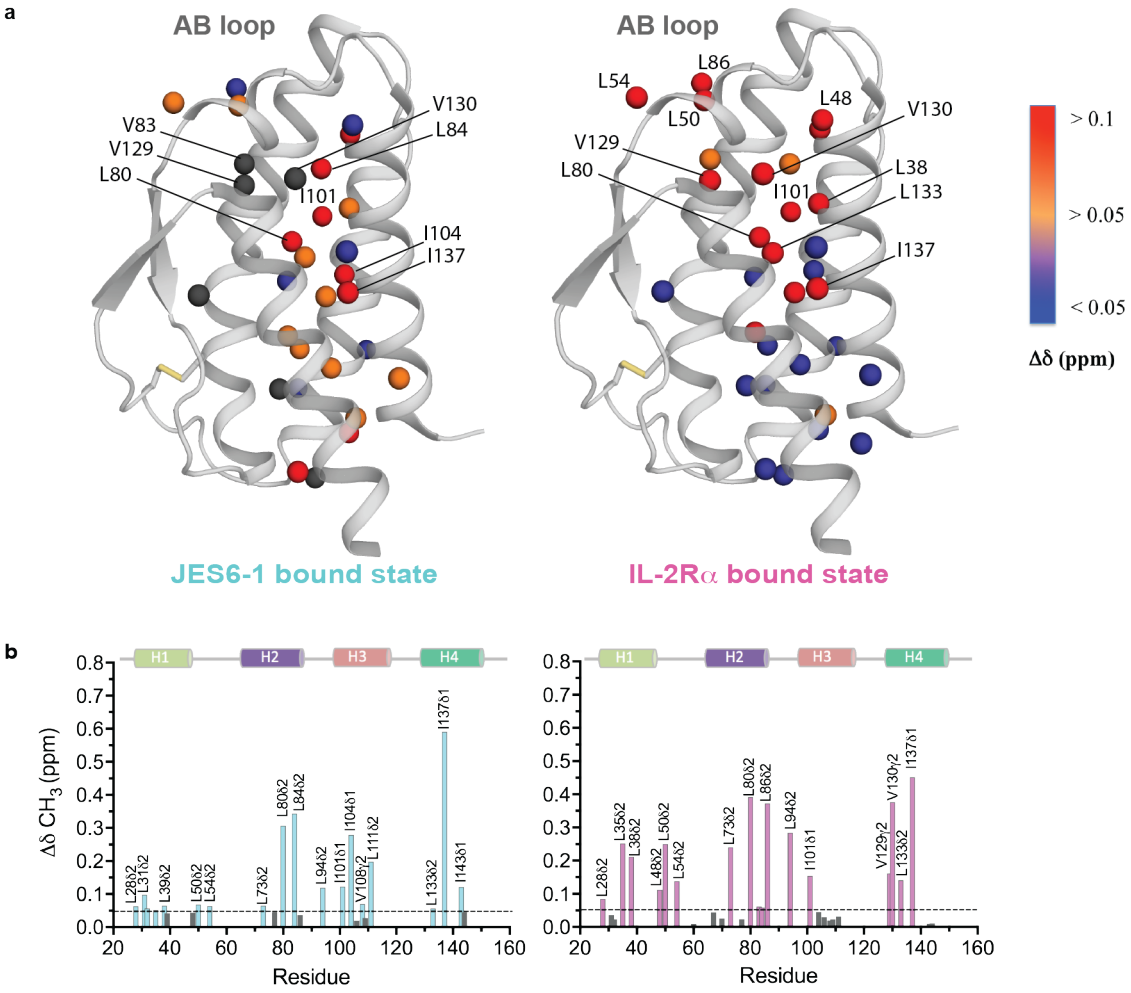

Supplementary Fig. 2 | Long-range effects in mIL-2 core dynamics induced by binding to the mIL-2Rα receptor or JES6-1 immunomodulatory scFv. (a) Effect of IL-2Rα receptor and JES6-1 scFv on the mIL-2 structure as assessed by chemical shift perturbation. The black spheres represent missing residues of mIL-2 due to significant exchange broadening upon JES6-1 binding. Chemical shift difference (Δδ, ppm) values are mapped by continuous-scale color onto the mIL-2 structure. (**b**) Histogram of chemical shift perturbations (Δδ) as a function of IL-2 residue number. Mapping of methyl chemical shift changes on the mIL-2 structure are shown in Figure 1. CSPs were calculated as described in Methods.

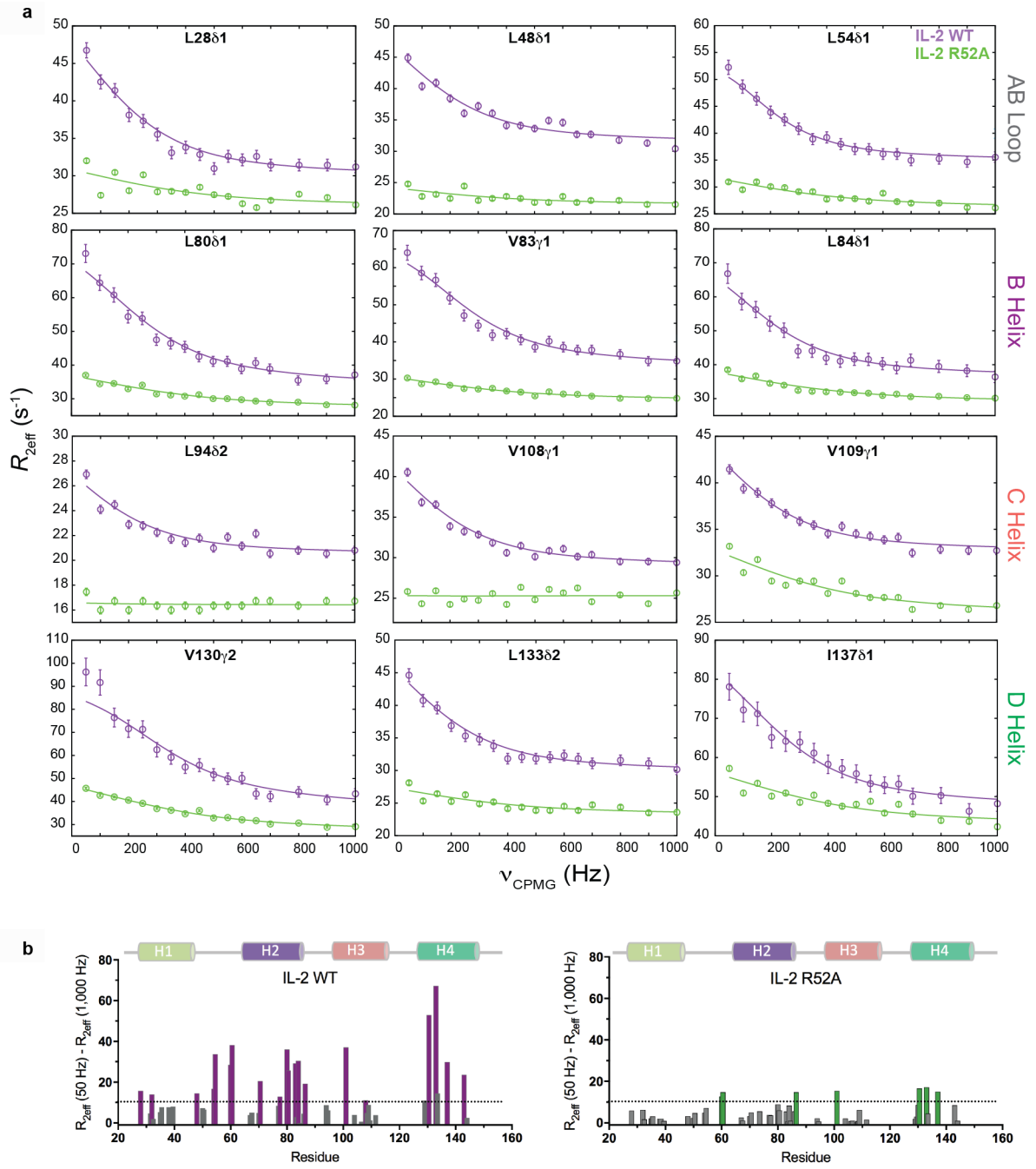

Supplementary Fig. 3 | Relaxation dispersion experiments indicate that R52A mutant abrogates conformational exchange in IL-2. (**a**) Experimental relaxation dispersion profiles (circles) for residues exhibiting µs-ms timescale dynamics as measured by ^{13}C SQ CPMG relaxation dispersion experiments for the WT (purple) and R52A (green) mIL-2, acquired at 600 MHz (25 ºC). Solid lines represent the best fit to a global two-site exchange model. Twenty residues of WT and R52A IL-2 were used for the global analysis using CATIA program. (**b**) Plots of the R_{ex} contributions of the methyl groups for WT and R52A mutant. R_{ex} contributions were calculated from the differences between R_{2eff} (50 Hz) and R_{2eff} (1000 Hz). The methyl groups with significant R_{ex} contributions (> 10 Hz) are colored purple for WT and green for R52A mIL-2.

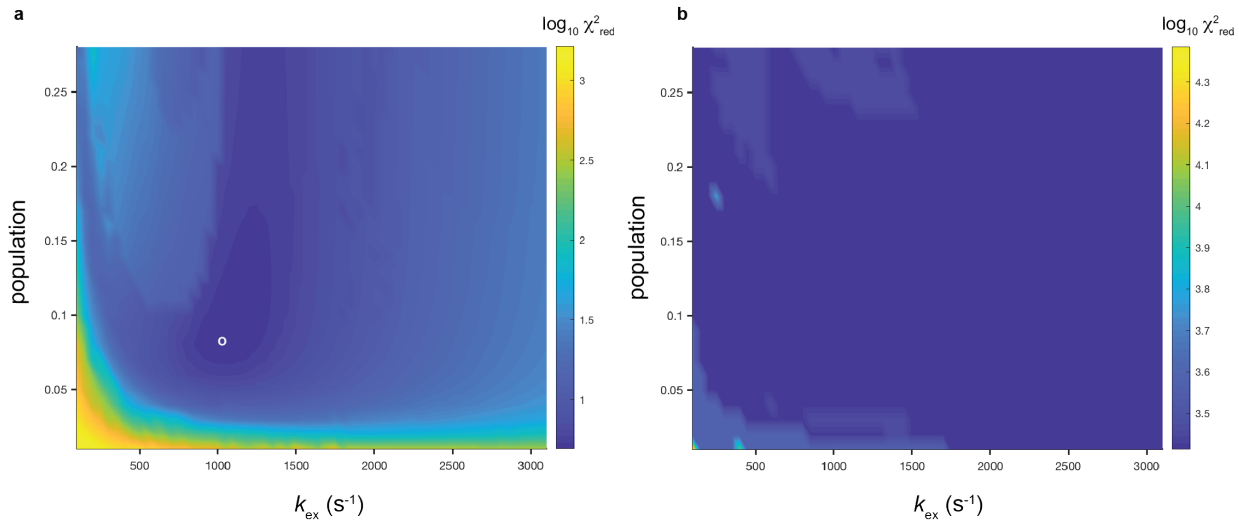

Supplementary Fig. 4| χ^2 surface plots generated from fits of CPMG relaxation dispersion data recorded at 600 and 800 MHz on ILV-methyl labeled mIL2 samples, WT (**a**) and R52A mutant (**b**). The |Δω| values were not fixed during the search for the minimum χ^2 value. The white circle indicates the position of (p_b, k_{ex}) that corresponds to the global minimum of χ^2.

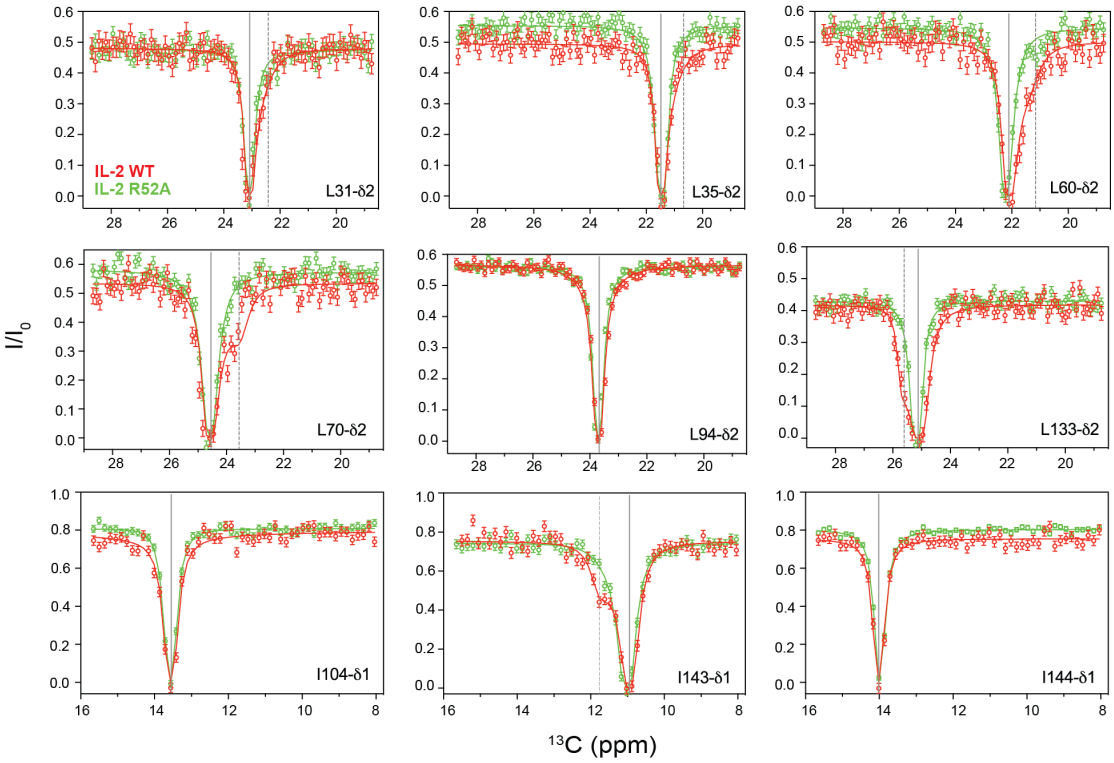

Supplementary Fig. 5 | R52A mutation disrupts the conformational dynamics of mIL-2 as measured by NMR. Representative of ^{13}C-CEST profiles obtained for WT (red) and R52A (green) mIL-2, recorded at a B_1 saturation field of 16.4 Hz (T_{CEST} = 300 ms), acquired at 800 MHz and 10 ºC. The chemical shift for the major state (solid lines) and minor state (doted lines) are indicated. Uncertainties in I/I_0 for CEST data are determined from the rmsd in the baseline of the profile where no intensity dips are present (typically, n > 30). L94, I104 and I144 are examples of residues in which a minor dip were not observed.

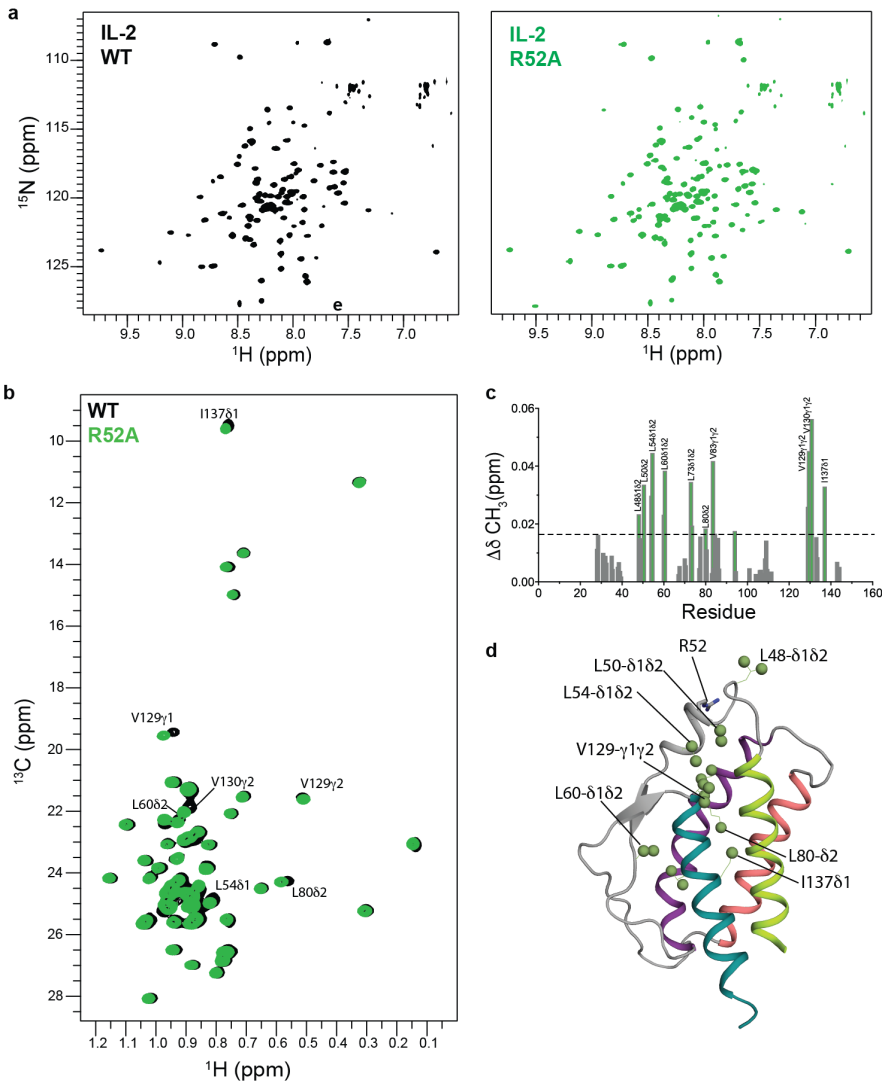

Supplementary Fig. 6 | ^{15}N and ^{13}C NMR characterization of R52A mIL-2. (a) Comparison of ^{1}H-^{15}N TROSY HSQC and (**b**) Superimposed ^{1}H-^{13}C-HMQC spectra of ILV-methyl labeled WT (black) and R52A (green) mIL-2, respectively. Assignments are indicated for residues with the largest chemical shift changes. Data acquired at 800 MHz, 25 ºC. (**c**) Histograms of chemical shift perturbations in ILV-methyl labeled IL-2. Residues with CSPs values 1s above the average are indicated (black doted line). CSPs were calculated as described in Materials and Methods. (**d**) Mapping of the methyl groups with marked chemical shift differences onto the mIL-2 structure. The results of the effect of this mutation on the dynamics of mIL-2 and binding to JES6-1 are shown in Figure 3.

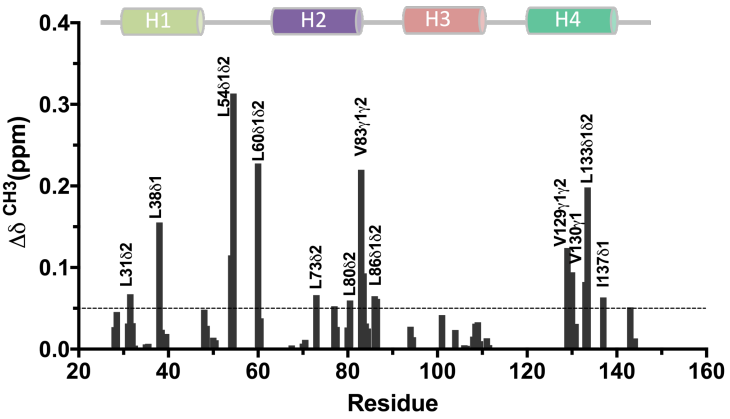

Supplementary Fig. 7 | Small molecule binding induces long-range effects and quenches dynamics in mIL-2. Histogram of chemical shift perturbations (Δδ) as a function of IL-2 residue number. Mapping of methyl chemical shift changes on the mIL-2 structure are shown in Figure 5. CSPs were calculated as described in Materials and Methods

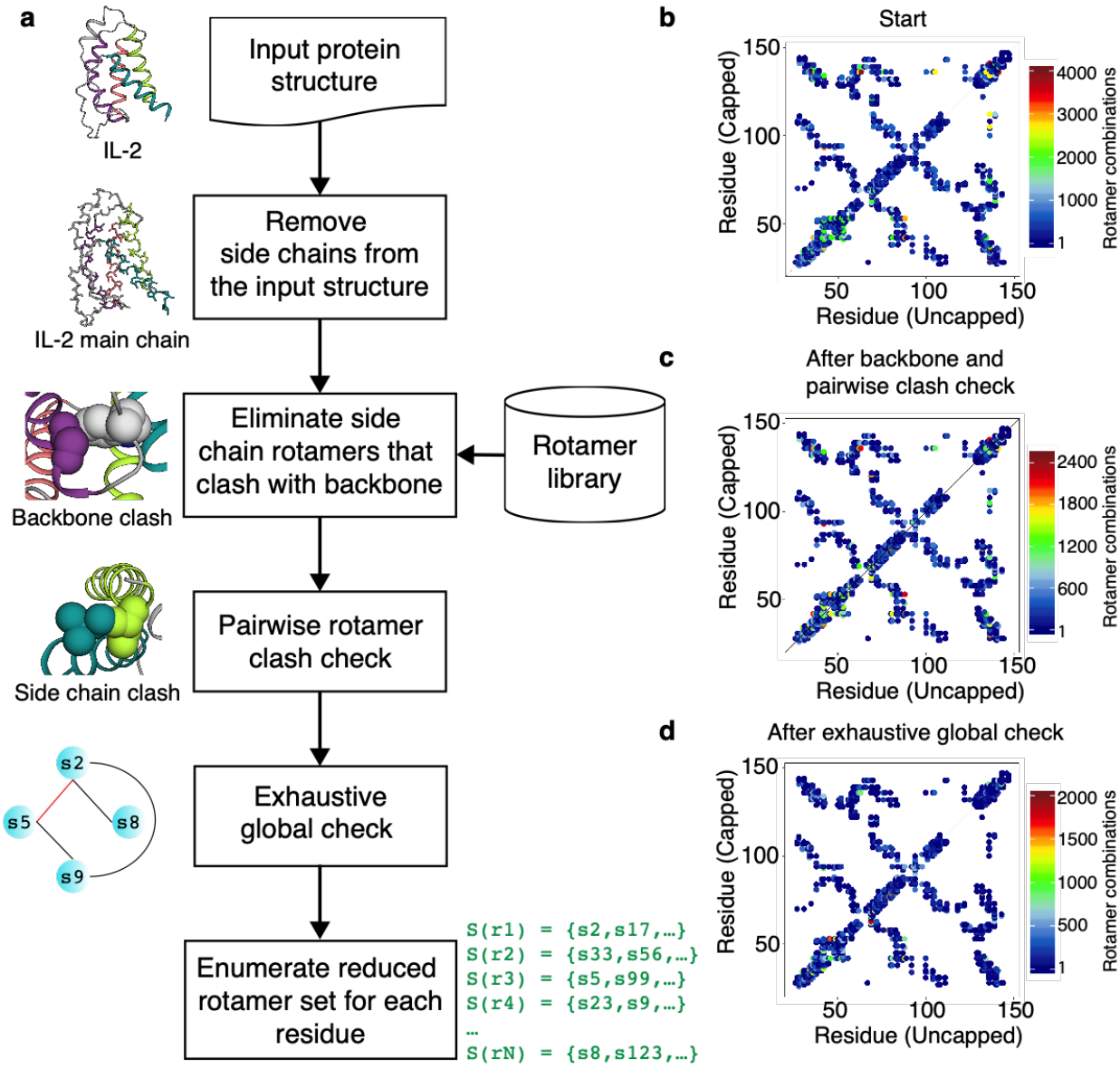

Supplementary Fig. 8 | (**a**) Workflow of the method used to perform side chain rotamer space analysis. (**b**) Number of rotamer combinations between neighboring residues along the sequence of IL-2. An upper bound for number of rotamer combinations after (**c**) backbone and pairwise clash check, and (**d**) exhaustive global check between neighboring residues. Here, the upper triangular matrix shows rotamer combinations for a capped structure, whereas the lower triangular matrix for an uncapped structure.

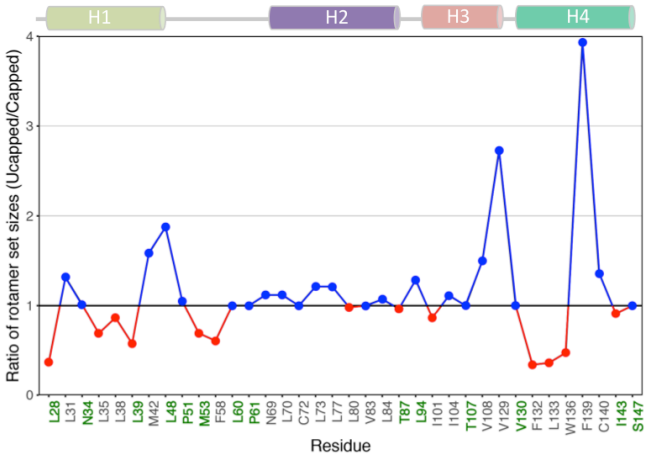

Supplementary Fig. 9 | Ratio of rotamer set sizes between the closed and open mIL-2 states. Blue/red points indicate residues showing expansion/contraction of allowed rotameric states in the uncapped structure. Black are residues that are buried in both capped and uncapped structures, and green residues that are buried in one of the two structures.

Supplementary Table 1 | Global fits of the ^{13}C-CPMG relaxation dispersion curves measured at 600 and 800 MHz at 25 ºC for WT mIL-2.

Residue	R_{ex} (600 MHz, s^{-1})	Δω (ppm)	p_B (%)	k_{ex} (s^{-1})
L28-Cδ_1	15.8	0.66 (0.02)	8.0 ±0.4	1,000 ±72
L35-Cδ_2	7.6	0.35 (0.03)		
L48-Cδ_1	14.5	0.53 (0.01)		
L54-Cδ_1	16.8	0.65 (0.23)		
L60-Cδ_1	28.5	0.99 (0.04)		
L60-Cδ_2	38.1	1.21 (0.08)		
L70-Cδ_2	20.6	0.66 (0.03)		
L80-Cδ_1	36.1	1.04 (0.03)		
L80-Cδ_2	25.7	0.78 (0.03)		
V83-Cγ_1	29.3	0.89 (0.03)		
L84-Cδ_1	30.4	0.85 (0.03)		
L86-Cδ_2	19.2	0.71 (0.02)		
L94-Cδ_2	6.2	0.34 (0.01)		
I101-Cδ_1	37.1	1.14 (0.04)		
V108-Cγ_1	11.1	0.48 (0.01)		
V109-Cγ_1	8.7	0.43 (0.01)		
V130-Cγ_2	52.9	1.53 (0.08)		
L133-Cδ_1	67.3	1.61 (0.09)		
L133-Cδ_2	14.4	0.55 (0.02)		
I137-Cδ_1	29.9	0.94 (0.05)		

***In order to justify group fitting, χ2group/ χ2local ≤ 2 where χ2local is the χ2 when a residue is locally fit and χ2 group is the χ2 of the same residue when group fit.**

Supplementary Table 2 | NOE violation analysis for the mIL-2 open and closed structures.

	Closed[b]	Open[c]
NOE distance constraint statistics		
Total NOE distance constraints[a]	26	26
Distance violations		
less than 1 Å	7	4
between 1 and 2 Å	1	2
between 2 and 5 Å	0	3
greater than 5 Å	0	7

[a] We used a strict upper distance bound up to 6 Å for the NOE restraints assigned manually.
[b] mIL-2 Rosetta homology model
[c] PDB: 4YQX

Supplementary Table 3 | Parameters obtained from the ITC experiments measured at 20 ºC.

Titrations	ΔG (kcal mol^{-1})	ΔH (kcal mol^{-1})	ΔS (cal K^{-1} mol^{-1})	Kd (nM)
WT mIL-2 + JES6-1	-11.6 ± 0.3	12.7 ± 0.1	83.1 ± 0.6	2
R52A mIL-2 + JES6-1	-7.8 ± 0.2	7.9 ± 0.3	53.8 ± 0.5	1557
R52A mIL-2 + IL-2Rα	-9.4 ± 0.2	-7.6 ± 0.2	6.1 ± 0.2	94

Supplemental Methods

mIL-2 NMR sample preparation, backbone and methyl assignments

The sequence encoding hexahistidine-tagged mouse IL-2 (mIL-2, amino acids 1-149) was cloned into the pMAL vector with an N-terminal maltose-binding protein (MBP) followed by a 3C protease site. U-[^{15}N,^{13}C,^{2}H]-labelled mIL-2 was overexpressed in *Escherichia coli* BL21(DE3) cells in M9 medium in $^{2}H_2O$ containing 2 g l^{-1} ^{2}H^{13}C glucose (Sigma #552151) and 1 g l^{-1} $^{15}NH_4Cl$. Selective methyl labelling with Ile-δ_1-[$^{13}CH_3$], Leu-δ-[$^{13}CH_3$/$^{12}C^2H_3$], Val-γ-[$^{13}CH_3$/$^{12}C^2H_3$], Met-ε_1[$^{13}CH_3$] referred to as MILV*, was achieved by the addition of appropriate precursors (ISOTEC Stable Isotope Products (Sigma-Aldrich) as detailed previously[1,2]. MILV-methyl (Ile $^{13}C\delta1$; Leu $^{13}C\delta1$/$^{13}C\delta2$; Val $^{13}C\gamma1$/$^{13}C\gamma2$; Met-$^{13}C\varepsilon_1$) U-[^{15}N, ^{2}H]-labelled mIL-2 was prepared in M9 medium in $^{2}H_2O$, supplemented with 2 g l^{-1} ^{2}H^{12}C glucose (Sigma #552003) and 1 g l^{-1} $^{15}NH_4Cl$. Both MILV* and MILV were induced at $OD_{600} \approx 0.7$ by addition of 1 mM IPTG and expression was performed for 20 h at 23 ºC. Protein in the periplasmic compartment was isolated by osmotic shock and purified by nickel-nitrilotriacetic acid (Ni-NTA) (Qiagen) affinity chromatography and via size-exclusion chromatography on a Superdex-75 column (GE Healthcare) in HEPES-buffered saline (HBS, 150 mM NaCl in 20 mM HEPES pH 7.0). NMR experiments were recorded at temperature of 25 °C using 14.0 and 18.8 T magnetic field, cryoprobe-equipped Varian and Bruker spectrometers, respectively. Both MILV* and MILV IL-2 samples contained 400 to 600 μM protein in 150 mM NaCl, 20 mM HEPES pH 7.0, 0.01% NaN_3, in 90% H_2O/10% D_2O. The backbone resonance assignments were obtained using a suite of TROSY-readout triple-resonance experiments[3] (HNCO, HNCA and HNCB) and subsequently extended to the Ile, Leu and Val sidechain methyls using a 3D HMCM[CG]CBCA methyl out-and-back experiment[4] recorded on the MILV* IL-2 sample. MILV sidechain methyl assignments were validated using methyl-to-methyl NOEs obtained from 3D H_M-C_MH_M SOFAST NOESY and 3D C_M-C_MH_M SOFAST NOESY experiments[5]. For the 3D H_M-C_MH_M SOFAST NOESY experiment, acquisition parameters were 40, 80, 1,024 complex points in the $^{1}H_M$, $^{13}C_M$, $^{1}H_M$ dimensions with corresponding acquisition times of 25, 10 and 80 ms with 4 scans/FID. For the 3D C_M-C_MH_M SOFAST NOESY acquisition parameters were 52, 32, 1,024 complex points in the $^{13}C_M$, $^{13}C_M$, $^{1}H_M$ dimensions with corresponding acquisition times of 13, 8 and 80 ms with 8 scans/FID. Backbone amide and sidechain methyl assignments were cross-validated using methyl-to-amide NOEs obtained from 3D H_N-C_MH_M SOFAST NOESY experiments[5]. The acquisition parameters were 64, 32 and 1,024 complex points in the $^{1}H_N$-$^{13}C_M$, $^{1}H_M$ dimensions with corresponding acquisition times of 15, 11 and 80 ms with 8 scans/FID. All 3D SOFAST NOESY experiments were recorded at 800 MHz, 25 °C on MILV-methyl-labelled mIL-2 samples using a recycle delay of 0.2 s and NOE mixing time of 300 ms. Assigned NOEs were cross-validated based on the Rosetta homology-based model of mIL-2 (using as a template PDB ID 1M47). In this manner, a set of complete assignments was obtained for the methyl groups of MILV (60) probes. All spectra were processed with NMRPipe[6] and analyzed with CcpNMR program[7].

Stereospecific isotopic labeling

A specifically methyl-labeled acetolactate precursor (2-[$^{13}CH_3$], 4-[$^{2}H_3$] acetolactate) was obtained through deprotection and exchange of the protons of the methyl group in position 4 of ethyl 2-hydroxy-2-(^{13}C)methyl-3-oxobutanoate (FB reagents) achieved in D_2O at pH 13[8]. Typically, 300 mg of ethyl 2-

hydroxy-2-(^{13}C)methyl-3-oxobutanoate was added to 24 mL of a 0.1 M NaOD/D_2O solution. After 30 min, the solution was adjusted to neutral pH with DCl and 2 mL of 1 M TRIS pH 8 in D_2O was added. For the production of highly deuterated [U-^{2}H], I-[$^{13}CH_3$]δ1, L-[$^{13}CH_3$]proS, V-[$^{13}CH_3$]proS WT mIL-2 samples, 300 mg/L of 2-[$^{13}CH_3$], 4-[$^2H_3$] acetolactate, prepared as described above, was added 1 h prior to induction (OD_{600} ≈ 0.55). 40 min later (i.e. 20 min prior to induction), 3,3-[$^2H_2$],4-[^{13}C]-2-ketobutyrate (SIGMA #589276) was added to a final concentration of 60 mg/L. Protein was induced at OD_{600} ≈ 0.7 by addition of 1 mM IPTG and expression was performed for 20 h at 23 ºC.

SEC MALS

Absolute molecular weight calculations were obtained by static light scattering in-line with size exclusion chromatography using a Wyatt Optilab T-rEX refractometer and mini DAWN Treos multiangle light scattering system at 4 ºC. mIL-2 protein samples (injection volume of 100 µL at 12mg/mL) were run at a 0.5 mL/min flow rate on a Superdex 200 10/300 GL gel filtration column (GE Healthcare) in a running buffer of 20 mM HEPES (pH 7.0), 150 mM NaCl. Protein concentrations were monitored by a refractometer and light scattering directly after the gel filtration column. Absolute molecular weights were determined using ASTRA version 6.0 (Wyatt Technologies).

Site-directed mutagenesis

pMAL-mIL-2 derivative plasmids carrying mutations were amplified using primers containing the mutations of interest and appropriate reverse primers using a Phusion polymerase (New England Biolabs) according to the manufacturer's recommendations. Template DNA was removed by Dpn I treatment, and transformed into *E. coli* DH5α strain. The introduced mutations and the absence of secondary mutations were verified by sequencing of plasmid DNA. Plasmids were transformed into *E. coli* BL21(DE3) strain.

mIL-2Rα receptor and JES6-1 scFv antibody samples preparation

mIL-2Rα (amino acids 1-213) ectodomain was secreted and purified using a baculovirus expression system, as previously described[9]. Recombinant JES6-1 single-chain Fv (scFv) was expressed and purified in a baculovirus expression system as described earlier[10]. All proteins were purified to >98% homogeneity with a Superdex 200 sizing column (GE Healthcare) equilibrated in 150 mM NaCl, 10 mM HEPES pH 7.3. Purity was verified by SDS-PAGE analysis.

STAT5 signaling

CTLL-2 cells (AATC TIB-214), a murine IL-2 dependent T cell line, were maintained in complete RPMI (RPMI 1640-glutaMAX supplemented with 10 % fetal bovine serum, non-essential amino acids, sodium pyruvate, 15 mM HEPES and penicillin-streptomycin supplemented with 1000 IU/mL recombinant mouse at 37 ºC with 5 % CO_2. Cells were rested in RPMI for 16 hours prior to signaling analysis. For STAT5 signaling, 2-3 x10^5 cells were cultured in 100 µL RPMI with cytokine or cytokine:antibody mixture (2:1) in a 96 well plate prior to fixation with 1.6 % paraformaldehyde for 10 min at room temperature. Cells were permeabilized with 100 % ice-cold methanol and stored at -20 ºC prior to staining. Cells were washed twice with FACS buffer (PBS pH 7.2, 2 % FBS, 2 mM EDTA) and stained with 1:100 Alexa Fluor 647 conjugated anti-STAT5

pY694 (BD) for 1 hour at room temperature. Mean fluorescence intensity (MFI) was monitored using a CytoFLEX flow cytometer (Beckman Coulter).

mIL-2Rα and JES6-1 NMR chemical shift mapping

2D ^{1}H-^{13}C SOFAST-HMQC were acquired on 100-200 μM Iδ_1-$^{13}CH_3$, L, V proS methyl-labelled mIL-2 in the free state and in the bound state in a 1:1 molar complex with IL-2Rα or JES6-1 at 800 MHz, 25 °C. Acquisition parameters were 256 and 1,024 complex points in the $^{13}C_M$, $^{1}H_M$ dimensions with corresponding acquisition times of 58 ms and 80 ms using a relaxation delay of 0.2 s with 8 scans/FID in the free state and 32 scans/FID in the bound state. The change in chemical shift (in p.p.m.) between the free and IL-2Rα or JES6-1 bound state of mIL-2 I(LV)proS-methyls was determined using the equation $\Delta\delta^{CH3} = [1/2\ (\Delta\delta^{2}H + \Delta\delta^{2}C/4)]^{1/2}$. To confirm the assignments of mIL-2 I(LV)proS-methyl peaks that shifted upon IL-2Rα binding, an additional 3D C_M-C_MH_M SOFAST NOESY was acquired on labelled mIL-2 in a 200 μM 1:1 complex with IL-2Rα using 45, 30, 1,024 complex points in the $^{13}C_M$, $^{13}C_M$, $^{1}H_M$ dimensions with corresponding acquisition times of 11, 7.5 and 80 ms and 48 scans/FID. The assignments of mIL-2 I(LV)proS-methyl peaks that shifted upon JES6-1 binding were confirmed by a 3D C_M-C_MH_M SOFAST NOESY using 45, 20, 1,024 complex points in the C_M-C_MH_M dimensions with corresponding acquisition times of 10, 4.5 and 80 ms and 32 scans/FID.

Small molecule NMR titration

The titration of the small molecule Ro 26-4550 (Tocris Bioscience) onto ILV methyl-labeled WT mIL-2 was performed on a 350 μM sample in NMR buffer (150 mM NaCl, 20 mM HEPES pH 7.2, 2.5% deuterated DMSO) at the following mIL2-Inhibitor ratios:
1:0, 1:0.04, 1:0.1, 1:0.2, 1:0.4, 1:0.7, 1:1, 1:1.2 and 1:4, with 2D ^{1}H-^{13}C SOFAST HMQC spectra as a readout. The mIL-2 sample was saturated (~97%) by the addition of a 4-fold excess of inhibitor. A small dilution of the protein sample occurred over the course of the titrations due to addition of the inhibitor solution aliquots. The compound was prepared as a 1mM stock solution in NMR buffer containing 2.5% deuterated DMSO. The change in chemical shift (in p.p.m.) between the free and Ro 26-4550 bound state of mIL-2 ILV-methyls was determined using the equation as described above. Data were processed with 4 Hz and 10 Hz Lorentzian line broadening in the direct and indirect dimensions, respectively and fit using a two-state model in TITAN[11] with bootstrap error analysis of 100 replicas. A total of eight NMR peaks were used for the global fitting procedure.

Methyl CPMG relaxation dispersion experiments

Methyl single-quantum ^{13}C CPMG relaxation dispersion experiments (Lundstrom et al., 2007) were recorded on highly deuterated ILV-methyl labeled WT and R52A mIL-2 samples (both at 400 μM protein concentration) at field strengths of 14.0 T and 18.8 T, at 25 ºC, using Varian and Bruker spectrometers, both equipped with a cryogenically cooled probe. The CPMG data set was acquired as pseudo 3D experiments with a constant relaxation time period T_{relax} of 20 ms and with 18 CPMG pulse frequencies $\nu_{CPMG} = 1/(2\tau)$ ranging from 50 to 1000 Hz, where τ is the delay

between the consecutive 180° refocusing pulses in ^{13}C CPMG pulse-train. Relaxation dispersion profiles $R_{2,eff}(\nu_{CPMG})$ were calculated from peak intensities (I) recorded at different CPMG frequencies ν_{CPMG} using the following equation: $R_{2,eff}(\nu_{CPMG}) = -1/T_{relax}\ln(I/I_0)$, where I is signal intensity in the spectra collected at T_{relax} = 20 ms, I_0 is signal intensity in the reference spectrum recorded at T_{relax} = 0. An interscan delay of 1.5 s was used with 24, 32 or 36 scans/FID, giving rise to net acquisition times between 40-58 h for a complete pseudo-3D data set. All data were processed using NMRpipe[6] and peak intensities were picked using CCPN[7]. The error was determined from the noise level of the spectra. The variation in $R_{2,eff}$ with ν_{CPMG} was fit to a two-state model of chemical exchange based on the Bloch-McConnell equations, to extract values of exchange parameters (p_B, $k_{ex}=k_{AB}+k_{BA}$), as well as ^{13}C chemical shift differences for nuclei interconverting between pairs of states. The software CATIA[12] was used to fit the data. Initially, global fits included 6 profiles for WT mIL-2 at two magnetic fields (L54δ1, L80δ2, V83γ1, L84δ1, I101δ1, L133δ1). The fitting was performed by minimizing the function χ^2 as previously described[13]. The group fit of selected residues was performed if the $\chi^2_{Group}/\chi^2_{Local}$ was less than 2.0. As a second step, 14 profiles (only from 14.0 T magnetic field) were used to obtain $|\Delta\omega|$ values calculated from per-residue and global fits with k_{ex} and p_B fixed to the values obtained in global data fits. For R52A mIL-2, analysis included 8 profiles at two magnetic fields (L60δ2, L80δ2, L84δ1, V109γ1, V129γ1, V130γ2, L133δ1, I137δ1).

χ^2 surface plot was generated for mIL-2 to evaluate the robustness of the extracted exchange parameters (pb, k_{ex}). Numerical fitting was performed using the CATIA program as before, with pb and k_{ex} sampled from a grid with values ranging from 0-30% and 0-3000 s^{-1}, respectively and $|\Delta\omega|$ was free to change during the χ^2 minimization procedure.

^{13}C CEST

^{13}C CEST experiments[14] were recorded on highly deuterated ILV-methyl labeled WT and R52A mIL-2 samples (both at 400 μM protein concentration) at field strength of 18.8 T at 10°C with an exchange period (T_{CEST}) of 300 ms and using a pair of B_1 fields, 16.2 and 32.4 Hz. For WT mIL-2, 135 data sets were obtained for B_1 = 16.2 Hz, with offsets ranging from 16 to 26 ppm (82 spectra, 25 Hz steps) and from 5.3 to 12.8 ppm (53 spectra, 30 Hz steps); 52 spectra were recorded from 16 to 26 ppm in 40 Hz increments for B_1 = 32.4 Hz. For R52A mIL-2, 135 data sets were obtained for B_1 = 16.2 Hz, with offsets ranging from 16 to 26 ppm (82 spectra, 25 Hz steps) and from 5.3 to 12.8 ppm (53 spectra, 30 Hz steps). Each 2D data set comprised of 60 (^{13}C) x 512 (^{1}H) complex points (28 ms, 64 ms), 16 scans/FID and a repetition delay of 2.0 s corresponding to a total measuring time of 88 (B_1 =16.2 Hz) and 63 (B_1 =32.4 Hz) h for each 2D series. Experiments were processed using NMRpipe[6] and CEST profiles were generated as the ratio in intensities of peaks in spectra acquired with and without the T_{CEST} period vs the position of the low power B_1 field. Uncertainties in I/I_0 were determined from the scatter in the baseline of CEST profiles where no intensity dips are present (typically, $n > 30$). Weak B_1 fields applied during T_{relax} were calibrated according to the procedure[15]. The CEST profiles were analyzed using the program Chemex

(https://github.com/gbouvignies/chemex), which numerically propagates the Bloch–McConnell equation as described[16]. Initially, data sets were analyzed simultaneously and all residues were included in the analysis, including those for which well-resolved excited state dips were not obtained. For the two-site exchange model, only residues that showed distinct major and minor dips or asymmetry were fit globally (nine residues) including the initial k_{ex} and p_b, and residue-specific $\Delta\omega$ values. As a third step, we fixed the global exchange parameters (k_{ex} and p_b) and re-fitted all residues.

Sidechain rotamer space analysis in mIL-2

We analyzed sidechain rotamer space of buried residues of mIL-2 using a customized software tool (**Extended Data Fig. 8a**). This software takes as input, a protein structure and then explores the sidechain rotamer space of the residues of interest. Before examining the space of rotamers, sidechains of the input structure are removed. Every sidechain rotamer of a residue obtained from a backbone dependent rotamer library is plugged in to check for a steric clash with its or its neighbors' backbones. All the rotamers that result in clashes with backbone are eliminated. Next, rotamers of neighboring residues are considered in pairs; clashing rotamer pairs are retained as constraints for subsequent step. The information about independent and pairwise rotamers is utilized towards an exhaustive global check phase that eliminates all the rotamers that are incompatible in all the valid combination of rotamers in a structure (**Extended Data Fig. 8b-d**). Finally, the reduced rotamer set for each residue is constructed and output by the tool.

Isothermal titration calorimetry

Titrations of WT and R52A mIL-2 (40 or 96 μM) into JES6-1 (4 or 9.6 μM) were performed at 20 °C, using a MicroCal VP-ITC instrument. To minimize enthalpy of solvation effects, all experiments were performed in phosphate buffer. All protein samples were extensively dialyzed against ITC buffer (20 mM sodium phosphate, pH 7.2, 150 mM NaCl). All solutions were filtered using membrane filters (pore size, 0.22 μm) and thoroughly degassed for 20 min before the titrations. Typically, two injections of 2 μL were followed by 26 injections of 10 μL until a molar ratio of 2.0-3.0 was obtained. The dilution heats are typically small and were subtracted from the calorimetric data. Integration of the thermogram and subtraction of the blanks yielded a binding isotherm that was fitted to a one-site binding model using the MicroCal Origin 7.0 software (OriginLab Corporation) to determine the stoichiometric ratios, the dissociation constants and the changes in enthalpy.

Supplementary References:

1. Tugarinov, V., Kanelis, V., Kay, L.E. Isotope labeling strategies for the study of high-molecular-weight proteins by solution NMR spectroscopy. *Nat. Protoc.* **1**, 749-754 (2006).

2. Natarajan, K., McShan, A.C., Jiang, J., Kumirov, V.K., Wang, R., Zhao, H., Schuck, P., Tilahun, M.E., Boyd, L.F., Ying, J., Bax, A., Margulies, D.H., Sgourakis, N.G. An allosteric site in the T-cell receptor Cβ domain plays a critical signalling role. *Nat Commun.* **8**, 15260 (2017).

3. Sattler, M., Schleucher, J. Heteronuclear multidimensional NMR experiments for the structure determination of proteins in solution employing pulsed field gradients. *Progress in Nuclear Magnetic Resonance Spectroscopy* **34**, 93-158 (1999).

4. Tugarinov, V., Kay, L.E. Ile, Leu, and Val methyl assignments of the 723-residue malate synthase G using a new labeling strategy and novel NMR methods. *J. Am. Chem. Soc.* **125**, 13868-13878 (2003).

5. Rossi, P., Xia, Y., Khanra, N., Veglia, G., Kalodimos, C.G. ^{15}N and ^{13}C- SOFAST-HMQC editing enhances 3D-NOESY sensitivity in highly deuterated, selectively [^{1}H,^{13}C]-labeled proteins. *J. Biomol. NMR* **66**, 259-271 (2016).

6. Delaglio, F., Grzesiek, S., Vuister, G.W., Zhu, G., Pfeifer, J., Bax, A. NMRPipe: a multidimensional spectral processing system based on UNIX pipes. *J. Biomol. NMR* 6, 277-293 (1995).

7. Vranken, W.F., Boucher, W., Stevens, T.J., Fogh, R.H., Pajon, A., Llinas, M., Ulrich, E.L., Markley, J.L., Ionides, J., Laue, E.D. The CCPN data model for NMR spectroscopy, development of a software pipeline. *Proteins* **59**, 687-696 (2005).

8. Gans, P., Hamelin, O., Sounier, R., Ayala, I., Durá, M.A., Amero, C.D., Noirclerc-Savoye, M., Franzetti, B., Plevin, M.J., Boisbouvier, J. Stereospecific isotopic labeling of methyl groups for NMR spectroscopic studies of high-molecular-weight proteins. *Angew Chem Int Ed Engl*. **49**, 1958-62 (2010).

9. Wang, X., Rickert, M., Garcia, K.C. Structure of the quaternary complex of interleukin-2 with its alpha, beta, and gammac receptors. *Science* **310**, 1159-1163 (2005).

10. Spangler, J.B., Trotta, E., Tomala, J., Peck, A., Young, T.A., Savvides, C.S., Silveria, S., Votavova, P., Salafsky, J., Pande, V.S., Kovar, M., Bluestone, J.A., Garcia, K.C. Engineering a Single-Agent Cytokine/Antibody Fusion That Selectively Expands Regulatory T Cells for Autoimmune Disease Therapy. *J Immunol.* **201**, 2094-2106 (2018).

11. Waudby, C.A., Ramos, A., Cabrita, L.D., Christodoulou, J. Two-dimensional NMR lineshape analysis. *Sci. Rep.* **6**, 24826 (2016).

12. Hansen, D.F., Vallurupalli, P., Lundstrom, P., Neudecker, P., Kay, L.E. Probing chemical shifts of invisible states of proteins with relaxation dispersion NMR spectroscopy: how well can we do? *J. Am. Chem. Soc.* **130**, 2667-2675 (2008).

13. McDonald, L.R., Boyer, J.A., Lee, A.L. Segmental motions, not a two-state concerted switch, underlie allostery in CheY. *Structure* **20**, 1363-1373 (2012).

14. Bouvignies, G., Kay, L.E. Measurement of proton chemical shifts in invisible states of slowly exchanging protein systems by chemical exchange saturation transfer. *J Phys Chem B* **116**, 14311-14317 (2012).

15. Guenneugues, M., Berthault, P., Desvaux, H.A. method for determining B1 field inhomogeneity. Are the biases assumed in heteronuclear relaxation experiments usually underestimated? *J Magn Reson* **136**, 118-126 (1999).

16. Bouvignies, G., Kay, L.E. A 2D ^{13}C-CEST experiment for studying slowly exchanging protein systems using methyl probes: an application to protein folding. *J Biomol NMR* **53**, 303-310 (2012).